

Observation of Charged Nanograins at Comet 67P/Churyumov-Gerasimenko

J. L. Burch¹, T. I. Gombosi², G. Clark^{3,4}, P. Mokashi¹, and R. Goldstein¹

¹ Southwest Research Institute, San Antonio, TX USA

² University of Michigan, AOSS Department, Ann Arbor, MI USA

³ Johns Hopkins University, Applied Physics Laboratory

Corresponding author email address: jburch@swri.edu

Author Manuscript

This is the author manuscript accepted for publication and has undergone full peer review but has not been through the copyediting, typesetting, pagination and proofreading process, which may lead to differences between this version and the [Version of Record](#). Please cite this article as doi: [10.1002/GRL.53313](https://doi.org/10.1002/GRL.53313)

Abstract

1
2
3 Soon after the Rosetta Orbiter rendezvoused with Comet 67P/Churyumov-
4 Gerasimenko at a solar distance of ~ 3.5 AU and began to fly in triangular-shaped
5 trajectories around it, the Ion and Electron Sensor detected negative particles at energies
6 from about one hundred eV/q to over 18 keV/q. The lower-energy particles came from
7 roughly the direction of the comet; the higher-energy particles came from approximately
8 the solar direction. These particles are interpreted as clusters of molecules, most likely
9 water, which we refer to as nanograins because their inferred diameters are less than one
10 hundred nm. Acceleration of the grains away from the comet is through gas drag by the
11 expanding cometary atmosphere while acceleration back to the vicinity of the comet is
12 caused partly by solar radiation pressure but mainly by the solar-wind electric field.
13 These observations represent the first measurements of energetic charged submicron-
14 sized dust or ice grains (nanograins) in a cometary environment.

15 16 **1. Introduction**

17 As a comet approaches the Sun, solar insolation produces an expanding atmosphere
18 through heating and sublimation of water vapor and other volatile elements and
19 compounds that were previously adsorbed on the surface of its nucleus or perhaps more
20 likely that originate below the surface. In the process, some of the smaller dust and icy
21 conglomerates on the surface are dragged away by the expanding atmosphere.
22 Photoionization by the Sun, particle impact by the solar wind, and collection of cometary
23 electrons produce a partially ionized gas with embedded dust and ice grains, i. e., an
24 expanding dusty plasma. Our interest here is in the smaller sized dust or ice grains, which

25 we refer to as nanograins (diameters of up to 100s of nanometers). The charge on the
26 grains is determined by photoemission, electron collection, and secondary emission
27 currents [cf. *Horányi and Mendis*, 1985]. At the large distance from the Sun of comet
28 67P/Churyumov–Gerasimenko (67P) during these observations (~3.5 AU) it might be
29 expected that electron collection dominates because of the $\sim R^{-2}$ dependence of solar UV
30 irradiance and solar wind flux [*Köhnlein*, 1996] combined with the generally $>100 \text{ cm}^{-3}$
31 electron densities observed close to the comet (~10 km), which decrease only linearly
32 with distance [*Edberg et al.*, 2015]. The grains should therefore be mostly negatively
33 charged, and this conclusion is possibly borne out by the fact that the spacecraft potential
34 during this phase of the mission was also generally negative [*Edberg et al.*, 2015; *Burch*
35 *et al.*, 2015].

36 As the nanograins are carried outward by the drag forces of the expanding atmosphere
37 they eventually reach a terminal velocity of a few hundred m/s at some tens of kilometers
38 above the comet [cf. *Gombosi et al.*, 1986; 2015]. From this point on, the nanograin
39 trajectories are influenced mainly by solar radiation pressure and the solar-wind electric
40 field (gravitational effects are negligible by comparison). Analysis of such trajectories by
41 *Horányi and Mendis* [1985] showed that solar radiation pressure produces parabolic
42 ballistic trajectories. These trajectories are modified by the solar wind electric field,
43 which becomes more important for smaller particles and less important for the larger
44 ones. Since radiation-pressure forces on the particles are conservative, they produce
45 simple reflection so that near the nucleus the returning particles have the same velocities
46 (the terminal velocities) they had when they left the comet. However, changes of the
47 charge state of the nanograins (e. g., by photoionization or electron collection) or of their

48 masses (e. g., by breakup) as suggested by *Gombosi et al.* [2015] could change the
49 energy/charge at which they are detected by an electrostatic analyzer.

50 In August 2014, *Rosetta* rendezvoused with comet 67P and commenced a series of
51 maneuvers that took it on two successive triangular paths (averaging 100 and 50
52 kilometers from the nucleus, respectively) whose segments are hyperbolic escape
53 trajectories alternating with thruster burns. The observations of charged nanograins
54 reported in this paper were made at cometocentric distances between 50 and 65 km on the
55 dayside of 67P between 23 August and 1 September 2014. **Figure 1** shows the trajectory,
56 the spacecraft position, and the directions to the Sun and comet on August 30, 2014 at
57 0613 UT, which is typical for all four events studied.

58

59 **2. Instrumentation and Data**

60 The Ion and Electron Sensor (IES) on the Rosetta Orbiter measures ions and electrons
61 with energy/charge from 4 eV to 18 keV with 8% energy resolution and $5^\circ \times 22.5^\circ$
62 angular resolution for electrons and $5^\circ \times 45^\circ$ for ions, with the ion sector normally
63 containing the solar wind segmented into nine $5^\circ \times 5^\circ$ channels [*Burch et al.*, 2007].
64 Because of the low data rates available (~ 265 b/s in burst mode), averaging over adjacent
65 energy and/or angular channels is typically necessary. Since Rosetta is a three-axis
66 stabilized spacecraft with no scan platform, IES performs electrostatic scanning of its
67 intrinsic $5^\circ \times 360^\circ$ azimuthal field-of-view (FOV) over $\pm 45^\circ$ yielding sixteen 5°
68 elevation angle channels and a total FOV of 2.8π steradians. This geometry leads to a
69 fan-shaped field of view for zero elevation angle but to one that lies along the surface of a
70 cone for positive or negative elevation angles. IES is mounted on a corner of the

71 spacecraft with the symmetry axis of the toroidal tophat analyzers centered on a 45° angle
72 from the local spacecraft zenith in order to maximize viewing of both the solar wind and
73 the comet for most anticipated spacecraft orientations. While this objective is generally
74 achieved, there are unavoidable obstructions for some azimuths at certain elevation
75 angles that graze the spacecraft. These obstructions are kept in mind and avoided during
76 data analysis.

77

78 3. Observations

79 **Figure 1(a)** shows the triangular-shaped trajectory of the Rosetta Orbiter (white trace)
80 along with lines from the comet to the Sun (yellow) and to the spacecraft (blue). **Figure**
81 **1(b)** shows a close-up view of a nucleus shape model with the same lines toward the Sun
82 and the spacecraft along with x (red), y (green), and z (blue) vectors in the J2000
83 coordinate system [Tapley et al., 2004]. **Figure 1** is typical for the four events studied
84 since for the entire period from August 23rd to September 1 the spacecraft was moving
85 slowly (a few m/s relative to the comet) along the same triangular path while staying on
86 the day side at comet distances between 50 and 60 km. In each case the line from the
87 comet to the spacecraft originates in the neck region of the comet from which plumes of
88 gas and dust have often been observed by the Rosetta navigation camera (e. g.,
89 <http://blogs.esa.int/rosetta/2014/10/02/cometwatch-26-km-on-26-september/>).

90 **Figure 2** shows energy-time spectrograms from the IES electron analyzer for (a)
91 August 25 and (b) August 30, 2014. On these days two adjacent energy channels, two
92 adjacent 5° elevation-angle channels and two adjacent 22.5° polar-angle (or azimuth)
93 channels were averaged in order to fit the available telemetry rate. The spectrograms plot

94 $\log_{10}(\text{counts}/0.38 \text{ s})$ at 62 energy steps. For an electrostatic analyzer like IES count rate is
95 proportional to energy flux. These two events are typical of the four events analyzed in
96 this study.

97 The events of interest occur between 05 and 06 UT in **Figure 2(a)** and between 06 and
98 07 UT in **Figure 2(b)**. In each case the upper spectrogram (from anodes 8 and 9) shows
99 high counts at energies extending up to the maximum observed by IES (18 keV/e). At
100 these same times similar signals, but at much lower energies (a few hundred eV), are
101 observed in anodes 0 and 1. As will be shown by **Figure 3**, anodes 8 and 9 look generally,
102 but not exactly, toward the Sun while anodes 0 and 1 view toward the comet in azimuth
103 but not in elevation angle, which can be up to 90° off the S/C – comet line.

104 **Figure 3** shows contour plots of energy flux for the nanograin events on 23, 25, and
105 30 August and 1 September 2014. All of these events are similar in that Rosetta was
106 positioned on the day side at 50 – 60 km from the comet. Each contour plot is for the
107 elevation angles for which the most energetic nanograin signal was most prominent.
108 Within the elevation-angle range plotted, the positions of the Sun and the comet along the
109 cone of observation are noted, as are the view angles of the 16 different polar-angle
110 anodes. As noted before, the angular scan of IES at a given elevation angle is not a 2D
111 fan except for the mid-range elevation angles. For the extreme elevation angles, e. g.,
112 channels 0 and 15, the angular scan is along the surface of the 45° half-angle cone [*Burch*
113 *et al.*, 2007]. In each of the contour plots in **Figure 3**, there is a strong signal at the
114 highest IES energies, which is located approximately at anode 8. The direction to the Sun
115 is positioned near anode 6 or 7 in each case. This angle of arrival of the negative particles
116 with respect to the solar direction is similar to that observed for pickup ions near comet

117 67P [Goldstein *et al.*, 2015], which is interpreted as resulting from the orientation of the
118 interplanetary magnetic and electric fields. This observation suggests that pickup of the
119 nanograins by the solar wind is important in addition to the effects of radiation pressure
120 as described by Horányi and Mendis [1985]. Near the direction to the comet a signal at
121 energies of a few hundred eV is noted in each case just outside the black region, which
122 extends out to ~32 eV. This black region results from the exclusion of data at the lower
123 energies, which include high fluxes of solar wind and ionospheric or coma electrons. In
124 addition to the signal from the comet direction, similar signals are seen in each case in
125 anode 4, which views a direction intermediate between the comet and the Sun. It is
126 possible that these signals are associated with the IMF direction although this possibility
127 cannot be confirmed with the currently available data.

128 In order to aid visualization of the geometry of the observations, the look directions of
129 the 256 IES channels are shown in **Figure 4** (top panel). Also shown are the directions to
130 the Sun and the comet in the CSO (Comet Solar Orbital) coordinate system (right-handed
131 system with origin at the comet, 0° longitude toward the Sun, latitude measured
132 northward from comet orbital plane, which is inclined by 7.05° to the ecliptic plane). The
133 data points shown in the middle and bottom panels of Figure 5, which locate the centers
134 of the fields of view of each channel are color-coded by the mean count rate over selected
135 energy/charge ranges--70 eV to 400 eV in the middle panel and 5 keV to 17 keV in the
136 bottom panel. Figure 5 shows that the lower-energy nanograins (in the 100 eV range)
137 were arriving from a narrow range of CSO longitudes aligned with the position of the
138 comet. However, the grains arrive over a wide range of latitudes, and the energy
139 dependence of the latitude variation is explored in the next paragraph. Figure 4 also

140 confirms that, as shown in **Figure 2**, the high energy particles arrived from roughly the
141 solar direction but offset from it as would be expected for particles picked up and
142 energized by the solar wind.

143 Energy spectra of the negative particles for the observations on August 25 for
144 elevation channels 0-1 and anodes 8-9 (approximately coming from the Sun) and anodes
145 0-1 (coming approximately from the comet in CSO longitude but inclined in latitude as
146 shown in **Figure 4** are shown in **Figure 5** (left-hand panel). The heavy trace is for
147 negative particles coming from the comet's longitude but displaced in latitude, while the
148 light trace shows particles coming from approximately the solar direction (see **Figure 4**).
149 While the returning particles (primarily picked up by the solar wind) show a broad,
150 mostly featureless energy spectrum extending through the highest IES energy channels,
151 the outflowing particles have lower energies with distinct peaks in the energy range
152 around 100 eV. These peaks are similar to those observed by *Hill et al.* [2012] in the
153 Enceladus plume that were interpreted to result from grains of different masses being
154 sampled by the rapidly moving Cassini spacecraft. If, as suggested by *Gombosi et al.*
155 [2015], the nanograins from the comet flow outward in a fairly narrow range of velocities
156 (a few hundred m/s) then the multiple peaks shown in **Figure 5** could possibly result
157 from particles with roughly equal masses and velocities but different charge states.

158 The right-hand panel of **Figure 5** shows the same heavy trace as in the left-hand panel
159 along with a light trace, which is the energy spectrum from anodes 0-1 at elevation
160 channels 14-15, which contain the direction closest to that of the comet. The same two
161 energy peaks in the 100 eV range appear in both traces but are at about 40% higher

162 energies in the heavy trace. The source of this latitudinal energy dependence is not
163 known but may be related to acceleration by the solar-wind electric field near the comet.

164

165 **4. Interpretation**

166 Although the data presented herein are from an electron analyzer, the presence of
167 fluxes at energies above 10 keV/e indicates that heavier particles such as negative ions or
168 charged nanograins (possibly clusters of ions) rather than electrons are being detected.
169 Solar wind electrons, photoelectrons, and coma electrons are all at much lower energies
170 (well below a few hundred eV). Because of the occasional and very localized nature of
171 the negative particle signatures and their point of origin in the neck region of the comet,
172 from which active plumes often originate, we conclude that they most likely are cometary
173 particles or grains that pick up electrons during their motion through the photoelectron
174 and coma electron environment close to the comet rather than atmospheric species
175 ionized by electron attachment (i. e., negative ions). This conclusion is further supported
176 by the fact that previous observations of negative ions from comets have been of thermal
177 ionospheric (coma) ions, which obtained their observed energies by the high velocity of a
178 flyby spacecraft such as Giotto [e. g., *Chaizy et al.*, 1991]. Moreover, since the terminal
179 velocity of dust or grains from the comet is expected to be a few hundred m/s [cf.
180 *Gombosi et al.*, 1986; 2015] the observed energies of particles coming from the nucleus
181 imply masses of $>10^5$ amu/e.

182

183 **5. Discussion and Conclusions**

184 The Rosetta IES data presented in this study represent the first measurements of
185 energetic charged submicron-sized dust or ice grains (nanograins) in a cometary
186 environment. Previous measurements of charged nanograins at Enceladus [Hill *et al.*,
187 2012] and at comet Halley [Sagdeev *et al.*, 1989] were of generally stationary particles
188 whose energies in the measurement frame resulted from high spacecraft velocities. For
189 Rosetta the very low velocities with respect to the comet (a few m/s) along triangular
190 trajectories 50-60 km from the comet in the sunward direction provided a unique
191 opportunity to observe charged nanograins ejected from the comet as well as their
192 predicted reflection by solar radiation pressure and solar-wind electric fields [Mendis and
193 Horányi, 2013; Mann *et al.*, 2014].

194 As Comet 67P and Rosetta complete their journey around the Sun and again move to
195 larger distances we anticipate more instances of the favorable triangular trajectories
196 upstream of the comet, which again will provide optimal viewing of nanograins as they
197 leave and return to comet 67P. During these future studies we expect to search for
198 collective plasma effects produced by the dust, perhaps including the dust acoustic waves
199 predicted by Rao *et al.* [1990], through their effects on electron densities. Another future
200 task we are considering is quantitative modeling of the solar-wind pickup process using
201 observed IMFs and solar-wind velocities to test the plausibility of this mechanism for
202 producing the accelerated and reflected grains.

203 These future observations may also provide opportunities to investigate possible
204 effects of the nanograins on ambient electron densities as suggested by Vigren *et al.*
205 [2015] and on the effects of nucleus charging on nanograin acceleration as proposed by
206 Szego *et al.* [2014]. These further measurements should also provide the opportunity to

207 search for interplanetary dust blown outward from the Sun as described by Mann et al.
208 [2014]. These particles have not been noticed as yet, possibly because their flux levels are
209 below the IES threshold or their energies are above the IES energy range.

210

211

212 **Acknowledgements.**

213 Rosetta is an ESA mission with contributions from its member states and NASA. The
214 data for this work are available from ESA's PSA archive or NASA's PDS Small Bodies
215 Archive. The work on IES was supported by the U.S. National Aeronautics and Space
216 Administration through contract #1345493 with the Jet Propulsion Laboratory,
217 California Institute of Technology. Work at the University of Michigan was
218 supported by NASA under contract JPL-1266313. We thank the teams at Imperial
219 College London and ESA who have been responsible for the operation of IES. Thanks
220 are due to ESA for providing the navigation camera images and the 3D nucleus
221 model and trajectory plots.

222

223

224

225

226 Burch, J. L., et al. (2007), RCP-IES: The ion and electron sensor of the Rosetta Plasma

227 Consortium, *Space Sci. Rev.*, doi: 10.1007/s11214-006-9002-4.

228 Burch, J. L., et al. (2015), Charge Exchange in Cometary Coma: Discovery of H⁺ Ions in

229 the Solar Wind Close to Comet 67P/Churyumov-Gerasimenko, in press, *Geophys.*

230 *Res. Lett.*

223 **References**

231 Chaizy P., et al. (1991), Detection of negative ions in the coma of Comet
232 P/Halley, *Nature*, 349, 393-396.

233 Coates, A. J., et al. (2007), Discovery of heavy negative ions in Titan's ionosphere,
234 *Geophys. Res. Lett.*, 34, L22103, doi: 10.1029/2007GL030978.

235 Edberg, N. J. T., et al. (2015), Spatial distribution of low-energy plasma around comet
236 67P/CG from Rosetta measurements, *Geophys. Res. Lett.*, 42,
237 doi:10.1002/2015GL064233.

238 Goldstein, R., et al. (2015), The Rosetta Ion and Electron Sensor (IES) Measurement of
239 the Development of Pickup Ions from Comet 67P/Churyumov-Gerasimenko,
240 *Geophys. Res. Lett.*, 42, 3093–3099, doi: 10.1002/2015GL063939.

241 Gombosi, T. I., A. F. Nagy, and T. E. Cravens (1986), *Rev. Geophys.*, 24, 667-700, doi:
242 10.1029/RG024i003p00667.

243 Hill, T. W., et al. (2012), Charged nanograins in the Enceladus plume, *J. Geophys. Res.*,
244 117, A05209, doi: 10.1029/2011JA017218.

245 Horányi, M., and D. A. Mendis (1985), Trajectories of charged dust grains in the
246 cometary environment, *Astrophys. J.*, 294, 357-368, doi: 10.1086/163303.

247 Köhnlein, W. (1996), Radial dependence of solar wind parameters in the ecliptic (1.1 R_{\odot}
248 - 61 AU), *Solar Phys.*, 169, 209-213, doi: 10.1007/BF00153841.

249 Mann, I., N. Meyer-Vernet, and A. Czechowski (2014), Dust in the planetary system:
250 Dust interactions in space plasmas of the solar system. *Physics Reports*, 536(1): 1-
251 39, doi: 10.1016/j.physrep.2013.11.001.

252 Mendis, D.A., and M. Horányi (2013), Dusty plasma effects in comets: Expectations for
253 Rosetta, *Rev. Geophys.*, 51, doi: 10.1002/rog.20005.

254 Rao, N., et al. (1990), Dust-acoustic waves in dusty plasmas, *Planet. Space Sci.*, 38, 543–
255 546, doi: 10.1016/0032-0633(90)90147-I.

256 Sagdeev, R. Z., et al (1989), Small-size dust particles near Halley’s Comet, *Adv. Space*
257 *Res.*, 9, 263–267, doi:10.1016/0273- 1177(89)90272-X.

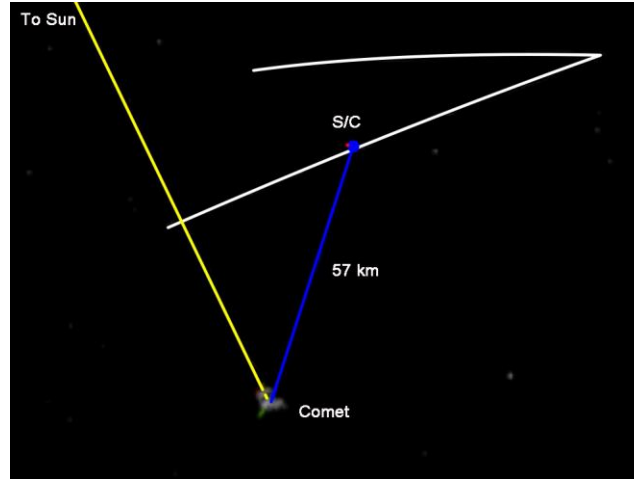
258 Szego, K., Juhász, A., & Bebesi, Z., (2014), Possible observation of charged nanodust from
259 comet 67P/Churyumov–Gerasimenko: An analysis for the ROSETTA mission, *Planet.*
260 *Space Sci.*, 99, 48.

261 Tapley, B. D., B. E. Schutz, and G. H. Born (2004), "Statistical Orbit Determination,"
262 *Elsevier Academic Press*, 29–32.

263 Vigren, E., et al. (2015), On the Possibility of Significant Electron Depletion due to
264 Nanograin Charging in the Coma of Comet 67p/Churyumov-Gerasimenko near
265 Perihelion, *Astrophys. J.*, 798, 130. doi:10.1088/0004-637X/798/2/130.

266

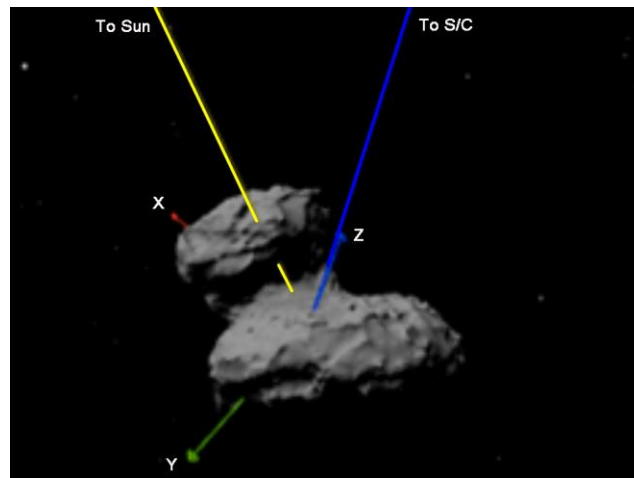
Author Manuscript



268

269

(a)



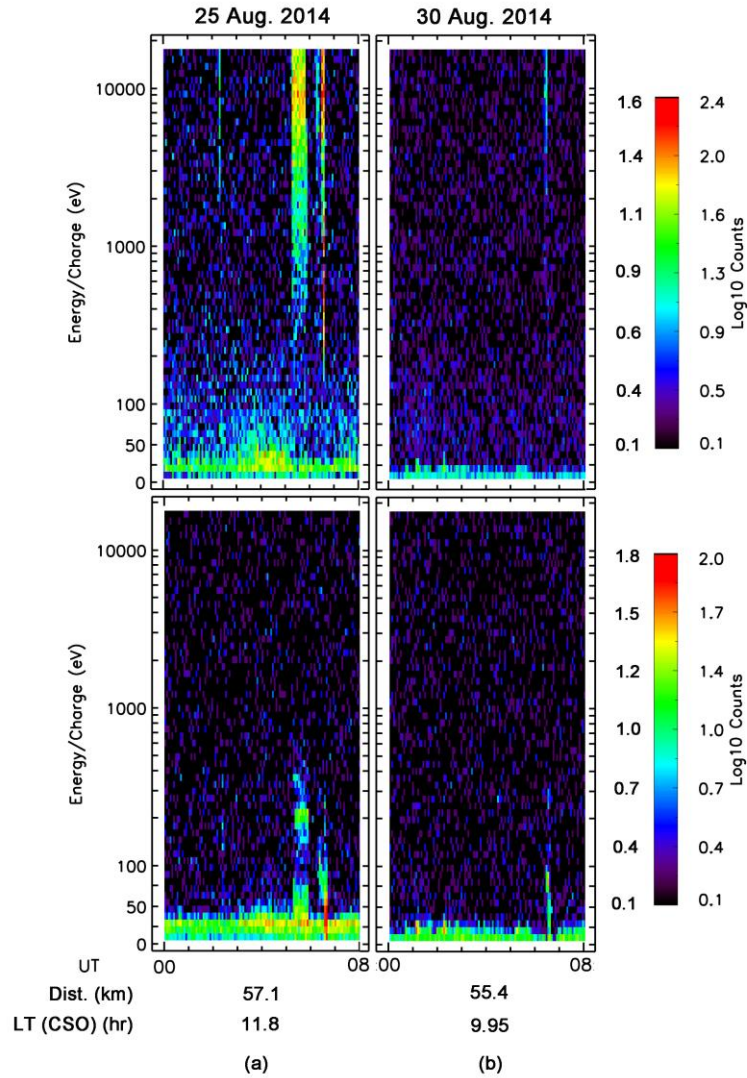
270

271

(b)

272 **Figure 1.** Position of Rosetta on 30 August 2014 at 0613 UT. (a) Triangular path of
 273 Rosetta (white), line to the Sun (yellow) and line to the spacecraft (blue). (b) Close-up
 274 view of the nucleus shape model showing lines to the Sun and the spacecraft along with
 275 cartesian vectors x (red), y (green), and z (blue) in the J2000 system (Heliocentric inertial
 276 frame at epoch Jan. 1, 2000). For scale, the comet-spacecraft distance is ~ 57 km and the
 277 long axis of the comet is ~ 5 km. Diagrams are provided by the “3d Tool” developed by
 278 the European Space Agency’s Rosetta Project.

Author Manuscript



280

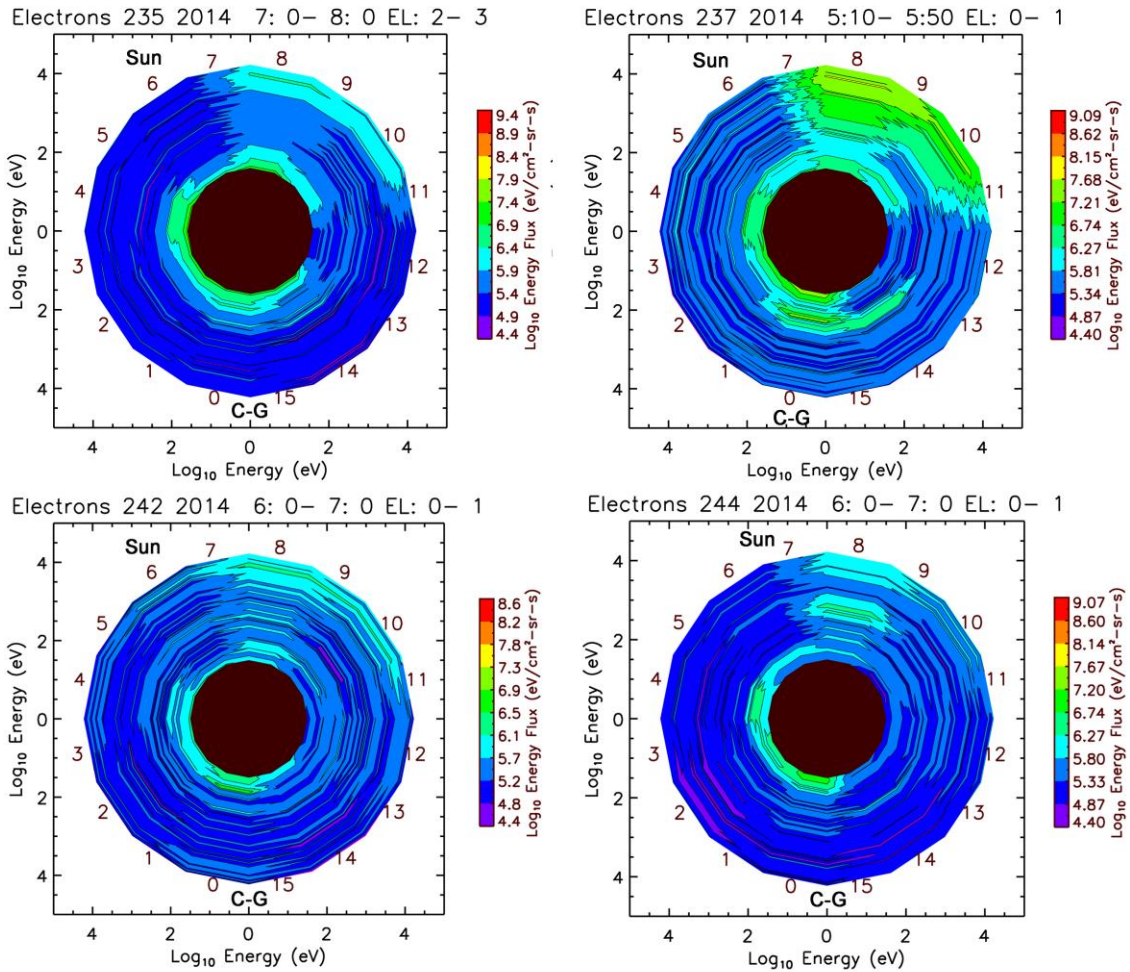
281 **Figure 2.** Energy-time spectrograms for negative particles on (a) August 25 and (b)

282 August 30, 2014. Data are from elevation angles 0 and 1 and for anodes 8 and 9 (top

283 plots) and anodes 0 and 1 (bottom plots). Count rates noted on the left and right hand

284 sides of the color bars are for 25 and 30 August, respectively.

285

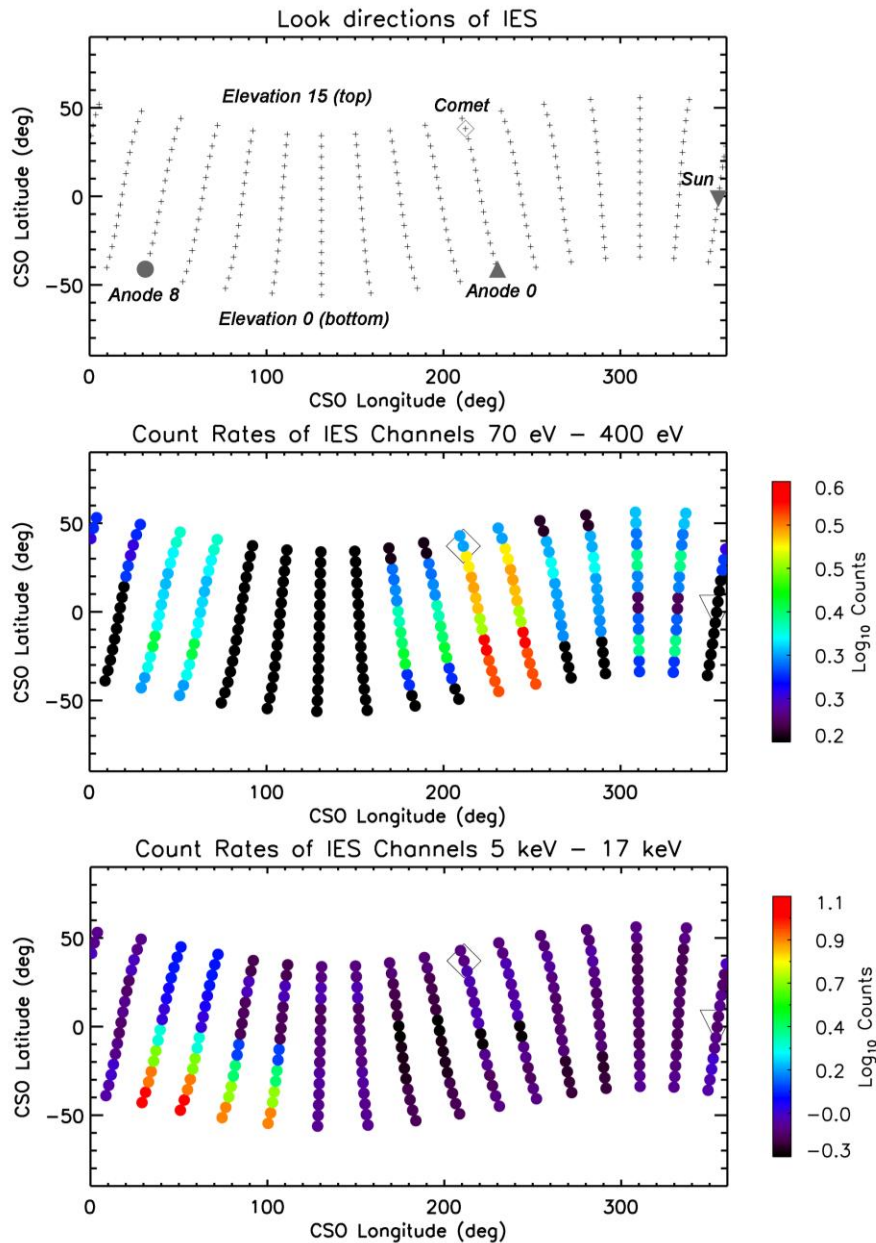


286

287 **Figure 3.** Contour plots of negative particle energy flux for one-hour periods on 23
 288 August (day 235), 30 August (day 242) and 1 September (day 244) 2014 and for a 40-
 289 minute period on 25 August (day 237) 2014. Anode numbers are noted along with
 290 notations of anode viewing angles toward the Sun and the comet (C-G).

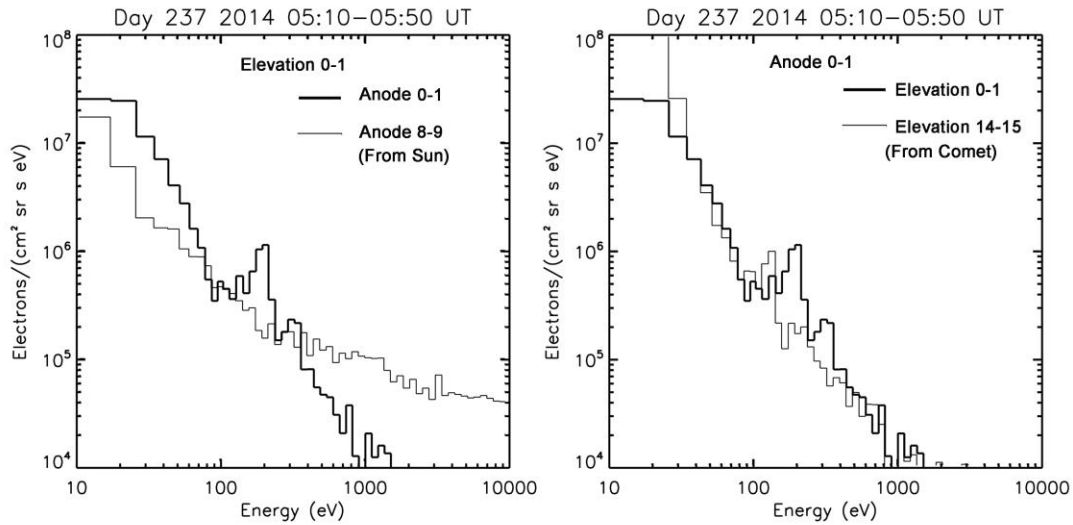
291

Author



293

294 **Figure 4.** *Top panel.* Viewing directions of the IES electron channels (elevation and
 295 azimuth) in the CSO (Comet Solar Orbital) coordinate system. *Middle and bottom panels.*
 296 Median counts per 0.38 s for each channel pair (adjacent elevation and azimuth channels
 297 are averaged) for the time period 05:10 to 05:50 UT on August 25, 2014 are shown by the
 298 colors of the data points, which are located at the center of each channel's field of view.



299

300 **Figure 5.** Energy spectra for negative particles (electrons below about 70 eV and
 301 nanograins for higher energies) (a) for two anode channels at elevation channels 0-1,
 302 which are shown in the contour plot in Figure 2 for day 237 (August 25) 2014 and (b) for
 303 two elevation channels at anode channels 0-1, which view in the direction of the comet at
 304 elevation channels 14-15.

305

Author Manuscript

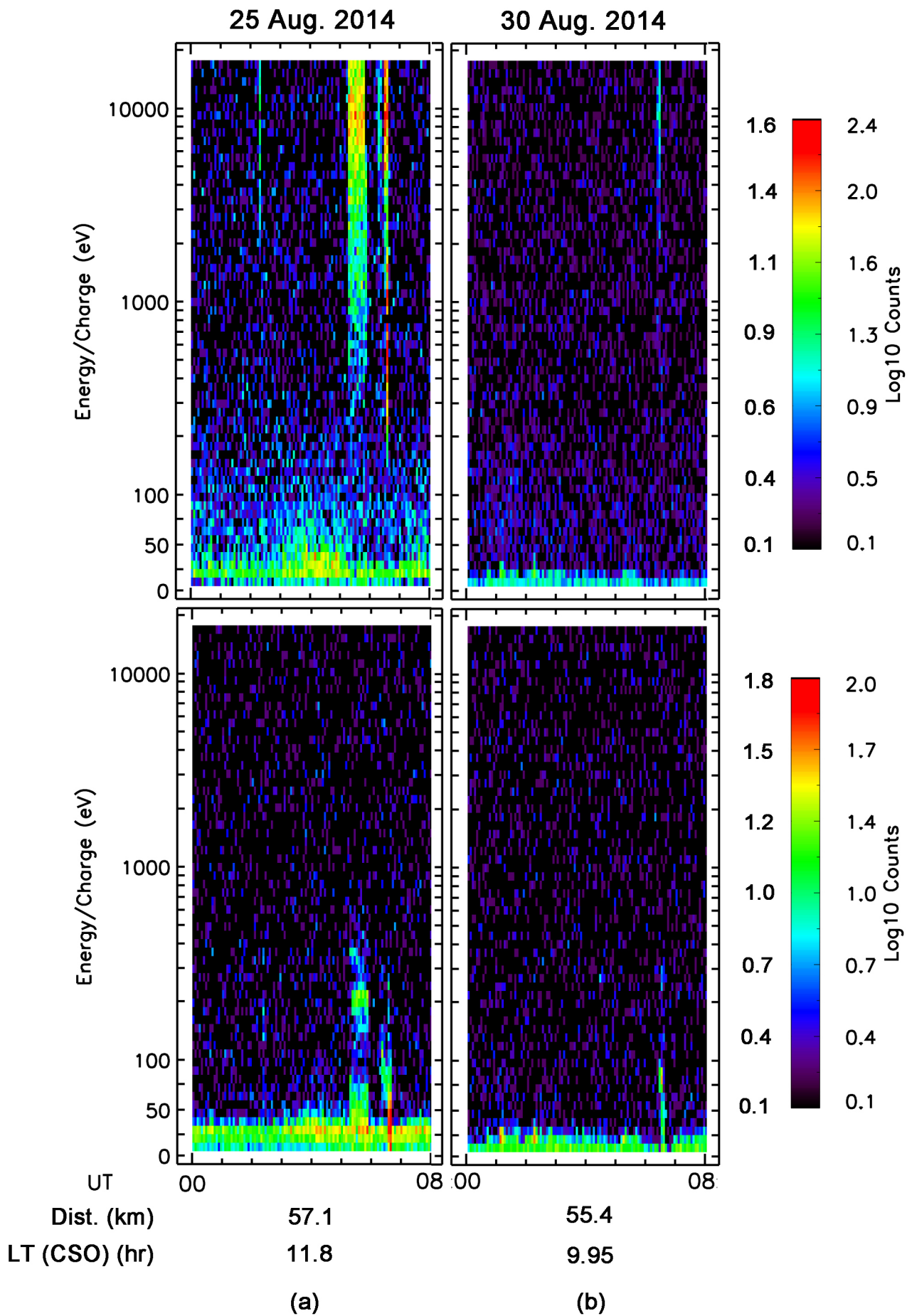


figure2.jpg

cript

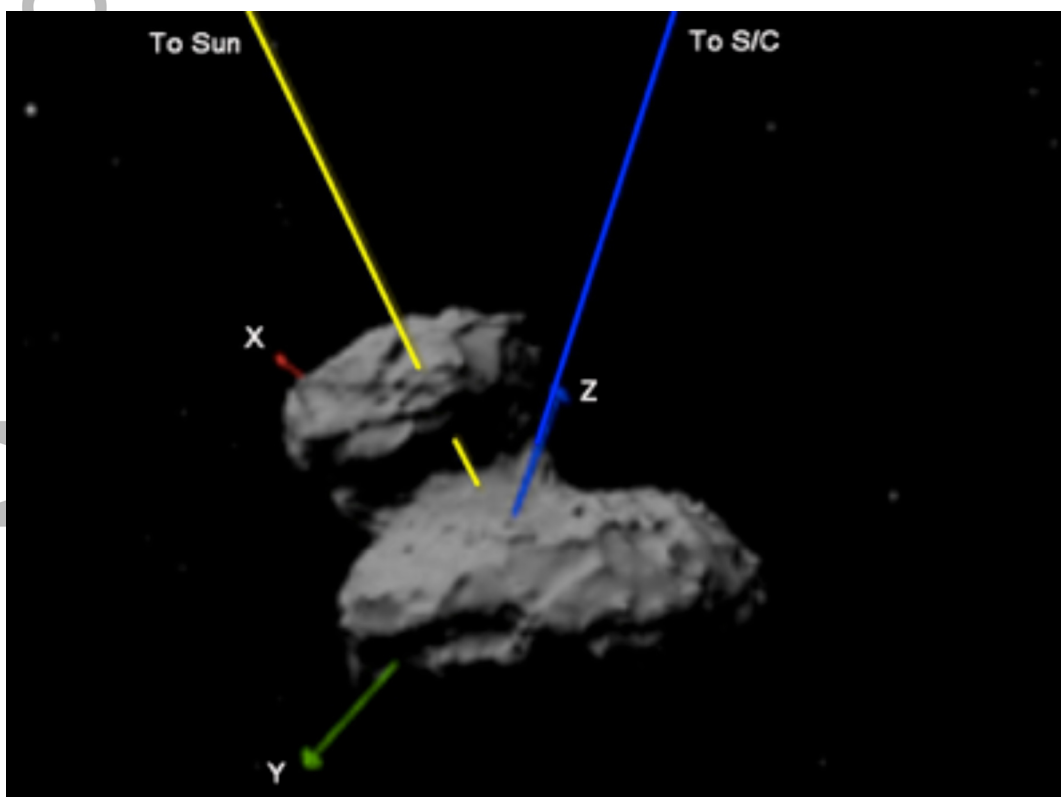
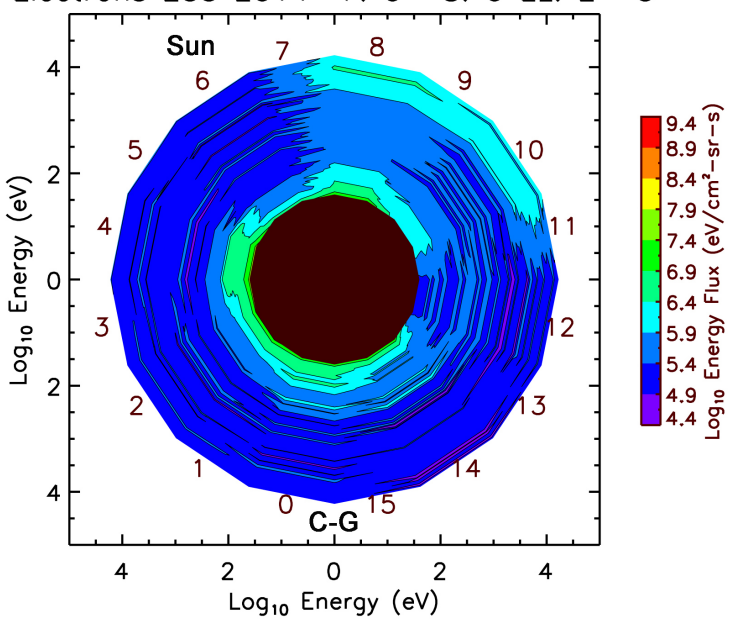


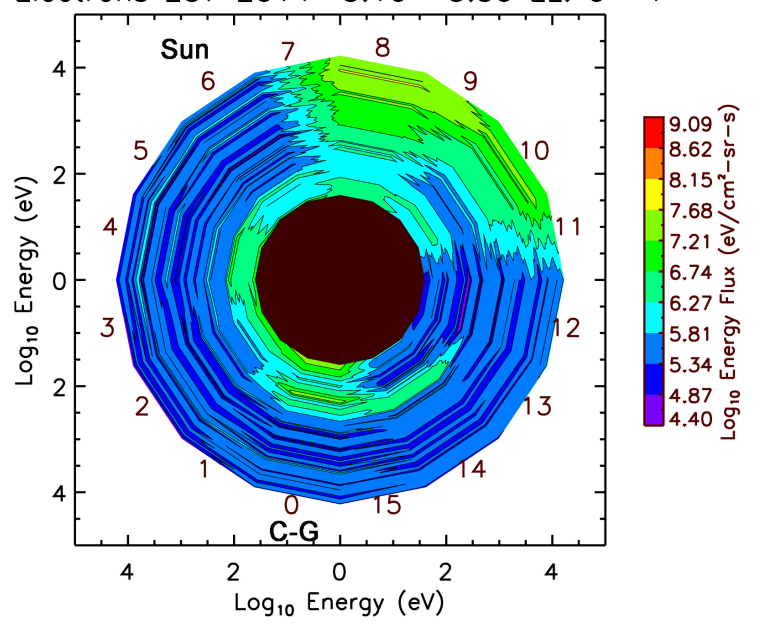
Figure1b.jpg

Autl

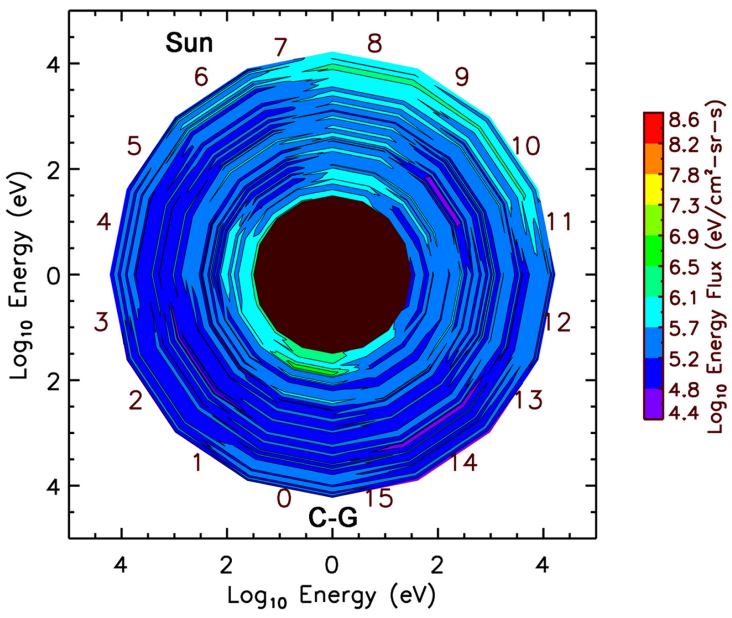
Electrons 235 2014 7: 0– 8: 0 EL: 2– 3



Electrons 237 2014 5:10– 5:50 EL: 0– 1



Electrons 242 2014 6: 0– 7: 0 EL: 0– 1



Electrons 244 2014 6: 0– 7: 0 EL: 0– 1

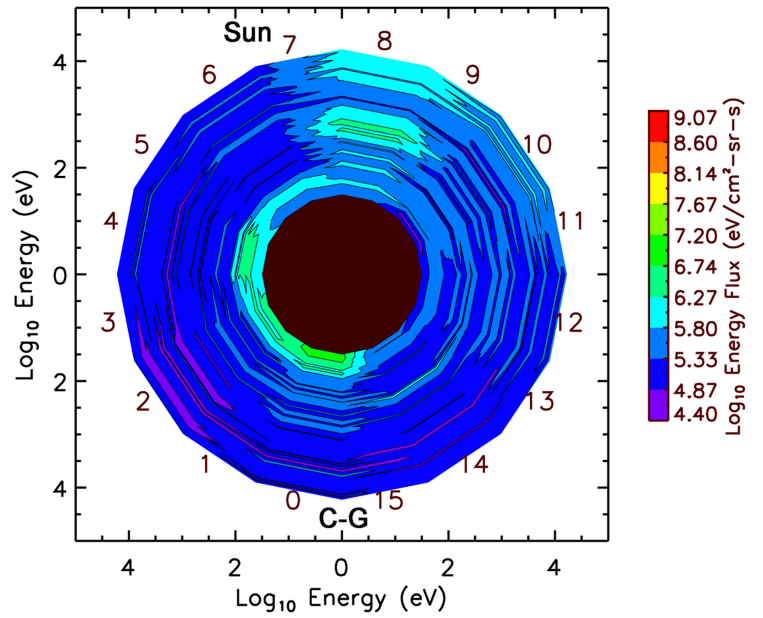


Figure3.jpg

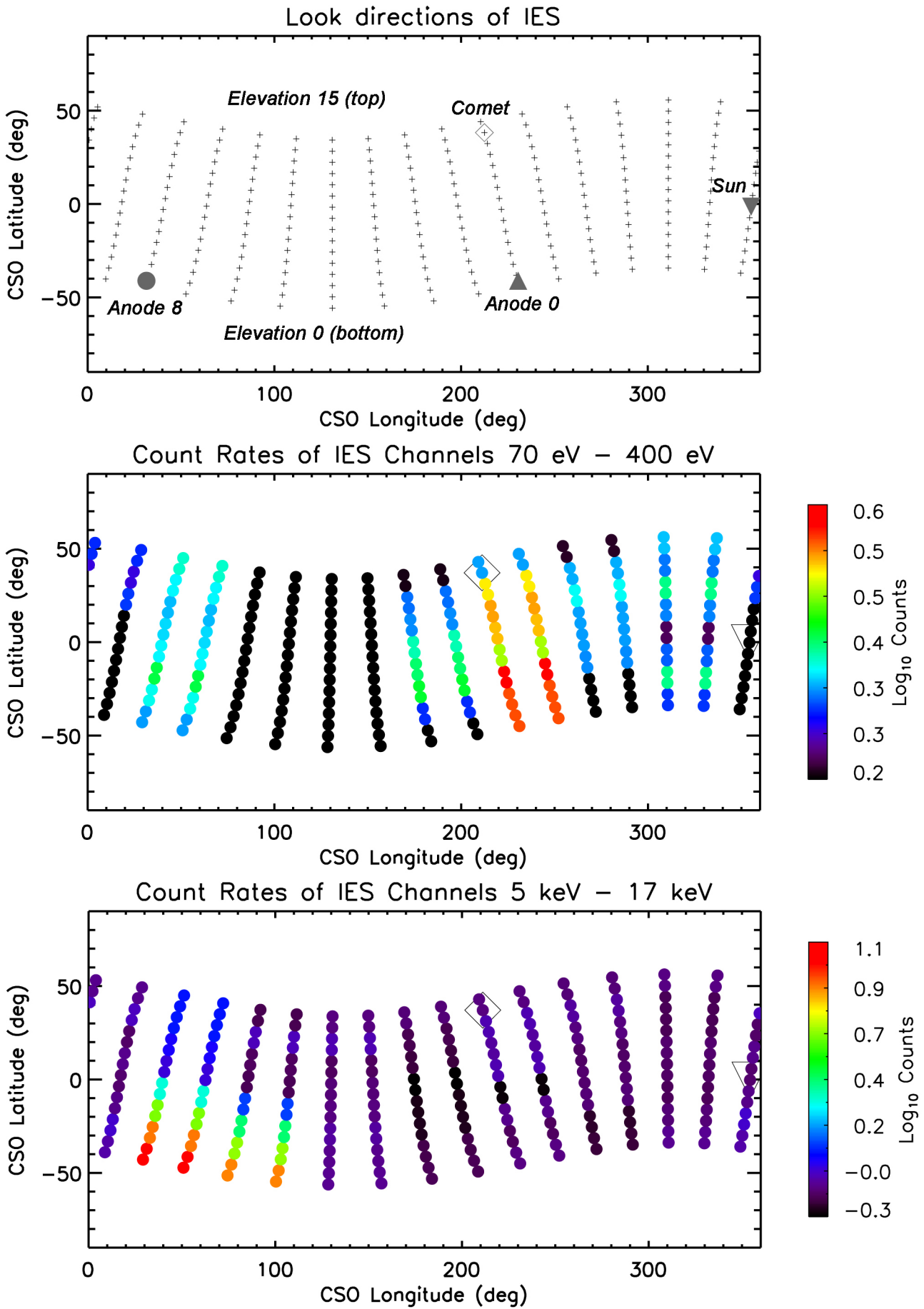
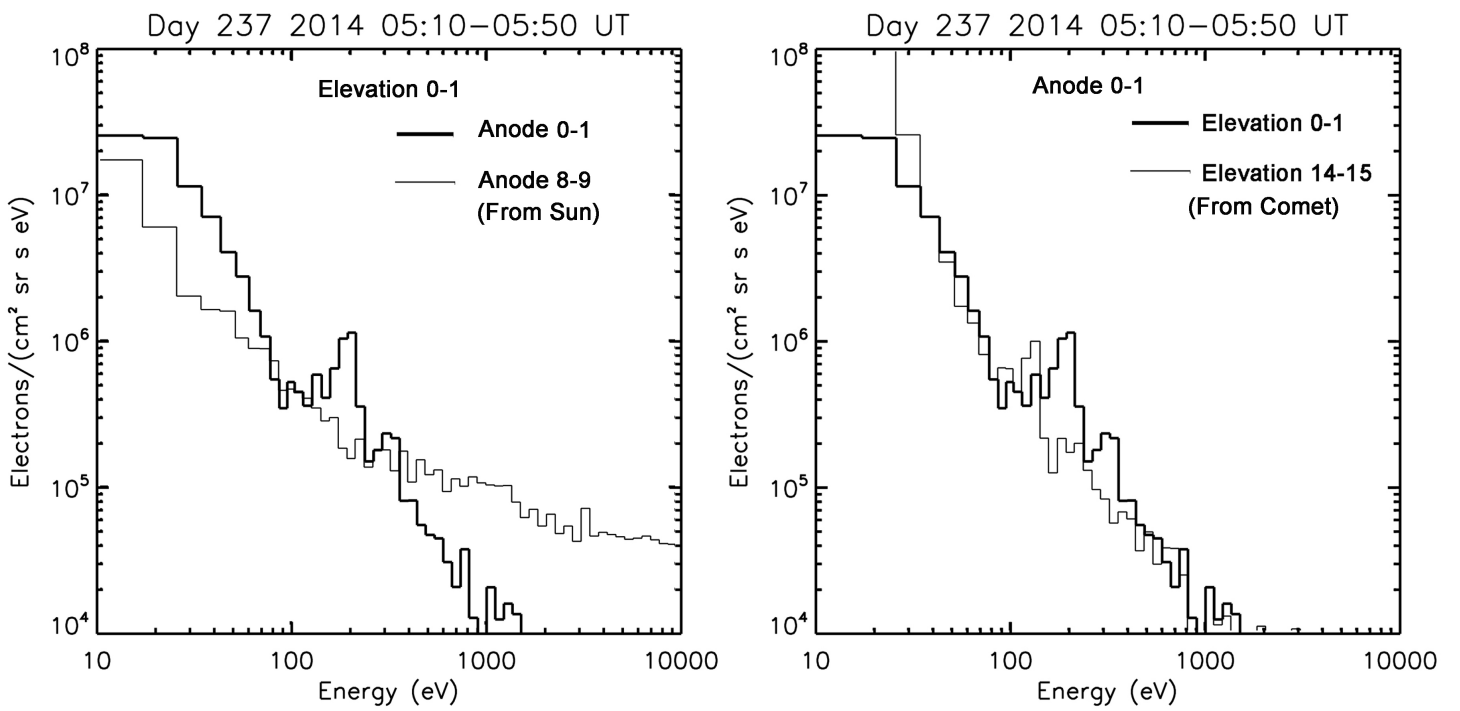


Figure4.jpg
 This article is protected by copyright. All rights reserved.

cript



Autl

Figure5.jpg

cript

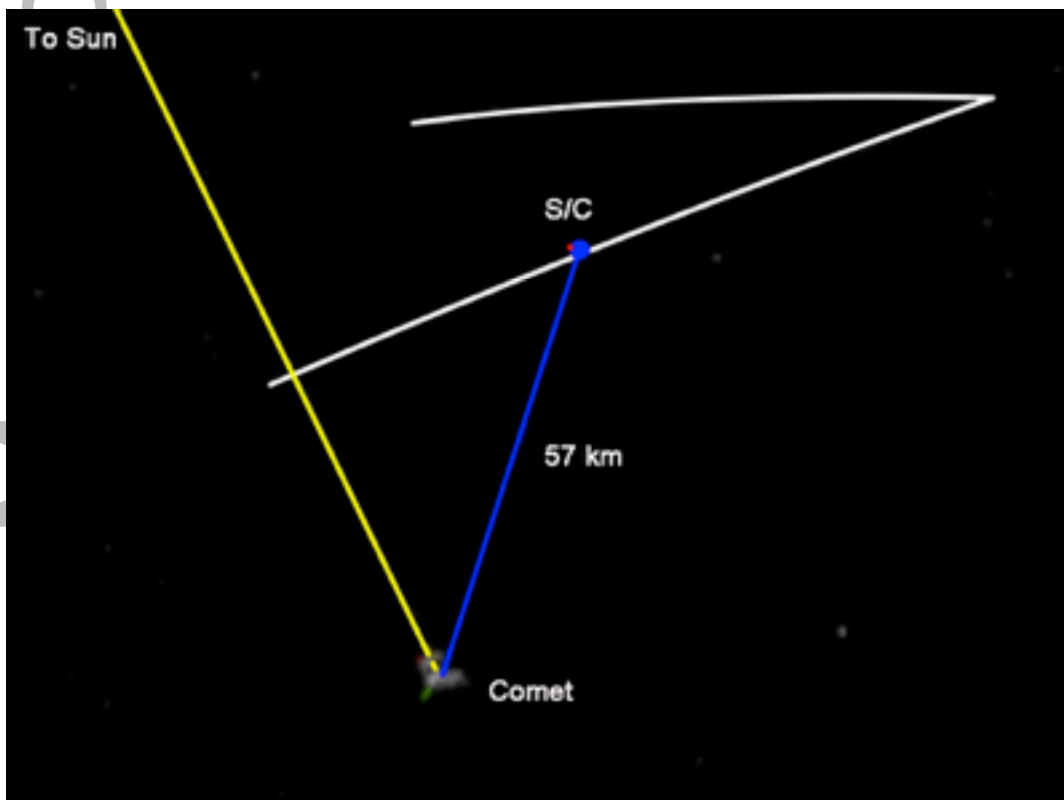


Figure 1a.jpg

Autl